Iranian Journal of Hydrogen & Fuel Cell 2(2015) 121-130

Iranian Journal of Hydrogen & Fuel Cell

IJHFC

Journal homepage://ijhfc.irost.ir

Synthesis of supported Pt alloy 3D rhombus shape nanoparticles for oxygen reduction reaction

Elaheh Lohrasbi[1], Mehran Javanbakht[1,2,*], Sayed Ahmad Mozaffari[3]

[1] Department of Chemistry, Amirkabir University of Technology, Tehran, Iran
[2] Fuel and Solar cell Lab, Renewable Energy Research Center, Amirkabir University of Technology, Tehran, Iran
[3] Department of Chemical Technologies, Iranian Research Organization for Science and Technology (IROST), Tehran, Iran

Article Information

Article History:

Received:
19 September 2015
Received in revised form:
02 December 2015
Accepted:
08 December 2015

Keywords

Graphene
PtFeCo alloy
3D rhombus shapes
Oxygen reduction reaction.

Abstract

In this study PtFeCo ternary alloy nanoparticles of three dimensional (3D) rhombus shapes dispersed on graphene nanosheets (PtFeCo/Gr) were successfully prepared and studied as electrocatalysts for the oxygen reduction reaction (ORR) in polymer-electrolyte fuel cells. A combination of analytical techniques including powder X-ray diffraction, X-ray photoelectron spectra, inductively coupled plasma-atomic emission spectrometry, scanning electron microscopy and electrochemical methods have been used for characterization of the synthesized electrocatalysts in this study. For comparison the graphene supported PtFe catalyst (PtFe/Gr), graphene supported PtCo catalyst (PtCo/Gr) binary alloys and graphene supported Pt catalyst (Pt/Gr) were also synthesized and investigated under the same experimental conditions. From the electrochemical analysis, it was found that PtFeCo/Gr particles exhibited an obvious enhancement of ORR activity in comparison with pure Pt and binary alloys. The significantly improved EAS, ORR activity and cell performance is achieved by increasing the utilization of the PtCoFe/Gr electrocatalyst by increasing the three-phase boundary in the electrocatalyst layer.

1. Introduction

Transition metals have long been used as catalysts in the form of dispersions stabilized on carbon substrates such as graphite, carbon nanotubes, and graphene [1]. Recently, platinum alloy nanoparticles have been used as catalysts for the catalytic reduction of oxygen. It has been reported that the alloys of Pt with non-noble metals, such as Fe, Co and other transition metals have shown great promise to lower catalyst cost and improve the ORR activity [2-5]. Kheirmand et al. used a binary catalyst consisting of Pt/C and Fe_3O_4 nanoparticles for an electrocatalytic oxygen reduction reaction. They observed that adding Fe_3O_4 with the same ratio of Pt/C caused the best utilization of Pt for the oxygen reduction reaction [6]. Malheiro et al. investigated PtFe/C catalysts with an Pt:Fe composition of 50:50 and 70:30, and found that a

*Corresponding Author: Department of Chemistry, Amirkabir University of Technology, Tehran, Iran. Tel.: +98 2164542764; Fax: +9821 64542762.
E-mail address: mehranjavanbakht@gmail.com (M. Javanbakht).

Pt-rich surface has an enhanced ORR performance [7]. Ramaprabhu et al. synthesized Pt_3Co/MWNTs via a modified polyol reduction method. They reported enhanced catalytic activity for Pt_3Co/ MWNTs towards ORR [8].

Also, ternary catalysts of platinum have been one focus of study during the last two decades. Recent developments and preparation methods for the ternary catalysts are reported by Karuppannan et al. and Antolini et al. [9, 10].

Catalytic reactivity of metal particles is undoubtedly linked to the nature of the surfaces involved in the catalysis. Determining the particle shape and consequently the atomic arrangements in the crystal planes of the catalyst surfaces is essential to understand the whole phenomena of catalysis and the design of more "ideal" catalysts for different chemical transformations.

Graphene, a new two-dimensional carbon material, consisting of a perfect sp^2-hybridized carbon atoms hexagonal network, has attracted tremendous attention from the scientific community because of its unique properties over other carbon nanomaterials [11-14], including superior electrical conductivity [15], high specific surface area (~2600 $m^2\ g^{-1}$) [16], ultrathin thickness, high structural elasticity [17] and chemical stability [18].

Kakaei et al. used graphene oxide as an electrocatalyst support in a cathode of direct methanol fuel cell (DMFC). They observed a better performance for the cell using graphen oxide as the electrocatalyst support compared to Pt/C in DMFC [12]. Kheirmand et al. used reduced graphene oxide film as an electrocatalyst support. Their results showed the proper performance of this green synthesized catalyst for oxygen reduction reaction [13]. Rowshanzamir et al. synthesized nitrogen-doped graphene (NG) by a low temperature solvothermal process to use as catalyst supports for oxygen reduction reactions (ORR). They reported that the produced NG acted not only as a support but also as a catalyst and had good catalytic activity for the oxygen reduction reaction in alkaline media [14].

The synthesis of the 3D rhombus-shaped nanoparticles adds a new structure to the list of already known shapes, i.e., tetrahedra, icosahedra, and cubooctahedra of platinum alloy particles. The 3D rhombus particles have large surface-to-volume ratios and may prove to have significantly different reactivity in catalysis.

In this paper, the synthesis of 3D rhombus-shaped platinum alloy nanoparticles on the graphene substrate was reported. Physical and electrochemical techniques were used for characterizing the structure, the composition and the electrochemical active surface area of the prepared catalyst.

The catalyst was also studied for oxygen reduction reaction in a proton exchange membrane fuel cell (PEMFC). For comparison the graphene supported PtFe catalyst (PtFe/Gr), graphene supported PtCo catalyst (PtCo/Gr) and graphene supported Pt catalyst (Pt/Gr) were also synthesized and investigated under the same experimental conditions.

2. Experiments

2.1. Synthesis of supported Pt alloy nanoparticles

In a typical synthesis, Pt/Gr, $Pt_{2.9}Fe_1$/Gr, $Pt_{2.9}Co_{0.9}$/Gr, and $Pt_{2.9}Co_{0.022}Fe_{0.070}$/Gr were obtained by chemical reduction of metals on OH functionlized graphene. For this purpose, OH functionalization and surface activation of graphene was done before use [16]. Then, 471 mg of OH functionlized graphene (Graphene nanopowder) was mixed with 155 mg of $H_2PtCl_{6.6}H_2O$ (Aldrich, 0.3 mmol), 0.6 mg $CoCl_{2.6}H_2O$ (Aldrich,0.0025 mmol) and 1.5 mg $FeCl_2$ (Aldrich, 0.0075 mmol) followed by sonication for at least 15 min (525 mg OH functionlized graphene, 155 mg of $H_2PtCl_{6.6}H_2O$ (0.3 mmol), 19.9 mg $FeCl_2$ (0.1 mmol) for $Pt_{2.9}Fe_1$/Gr and 537 mg OH functionlized graphene, 155 mg of $H_2PtCl_{6.6}H_2O$ (0.3 mmol), and 23.8 mg $CoCl_{2.6}H_2O$ (0.1 mmol) for $Pt_{2.9}Co_{0.9}$/Gr). Subsequently, a solution of 0.1 M $NaBH_4$ was added and sonicated for at least 1 h to ensure the complete reduction of metals (the molar ratio of $NaBH_4$ to transition metal ions in the reaction mixture was 2:1 to ensure complete reduction of metal ions). Then, the mixture was transferred into an autoclave and heated

to 120°C and kept there for 24h. Finally, black supported Pt alloy nanoparticles precipitated at the bottom of the autoclave. The product was collected by centrifuge, washed and dried in a split-hinge furnace at at 100 °C for an hour and then followed at 500°C for 60 min under constant flow of argon.

2.2. Structural and morphological studies

The synthesized supported Pt alloy nanoparticles were characterized by X-ray diffractometer (XRD) by a Philips PW1800 X-ray diffractometer using Cu Kα radiation operating at 40 KV and 20 mA.

An X-ray photoelectron spectrometer (XPS) equipped with an Al-K X-ray source operated at 1486.6 eV was employed to investigate the surface chemical composition of the films. A hemispherical energy analyzer (Specs EA 10 Plus) operating in vacumm better than 10^{-7}Pa was used to determine the core-level binding energies of photoelectrons emitted from the surface. All of the peaks were deconvoluted using the SDP software program (version 4.1) with 80% Gaussian–20% Lorentzian peak fitting. All binding energy (BE) values were calibrated by fixing the C1s core level with a BE of 285.0 eV.

The elemental composition was obtained with an IRIS advantage inductively coupled plasma atomic emission spectrometry (ICP-AES) system (Varian Austria).

A scanning electron microscope (SEM, Philips model XL 30) was used to characterize the morphology of the synthesized electrocatalysts.

2.3. Voltammetric measurements

Cyclic voltammetric (CV) measurements were carried out using an Autolab potentiostate/galvanostate (Metrohm, Netherland). Experiments were done in a conventional electrochemical cell holding 50 ml and three electrode system, consisting of a saturated Ag/AgCl electrode as the reference electrode, a modified glassy carbon electrode as the working electrode (20 µL of the suspension of the synthesized electrocatalysts with metal loading ~25 % in water/ethanol/5 wt% Nafion 1: 1: 0.02 were dropped onto glassy carbon rod), and a platinum wire as the auxiliary electrode. The temperature was maintained at 25.0 ± 0.5 °C, using a water thermostatic bath.

Single-cell PEMFC performance of the electrocatalysts was evaluated by homemade gas diffusion electrodes in a fuel cell test station (Paxi Tech FCT-150S). The gas diffusion layer was prepared according to the method described in [19]. In short, the carbon powder (Vulcan XC-72, Cabot Corp.), 30 wt.% of PTFE and ethanol were ultrasonically mixed with a ratio 13:7 of carbon to solid PTFE loading. The viscous mixture was coated onto the wet-proofed carbon paper (Toray Co, Jap.) with PTFE. The gas diffusion layer was dried, then baked for 30 min at 280 °C, and finally sintered at 330 °C for 30 min to prepare the micro-porous layer (MPL). Then, the electrocatalyst was painted onto the gas diffusion layer as a homogeneous suspension consisting of the required amount of the electrocatalysts, 33 wt. % Nafion (Aldrich, 5%) and isopropanol (Panreac), followed by drying in an oven at 140°C for 45 min. The electrocatalyst-loaded electrode with approximately 0.1 mg cm^{-2} Pt was used as the cathode, and a commercial 20 wt. % Pt/C electrode (E-TEK) was used as the anode with a Pt loading of 0.1 mg cm^{-2}.

The membrane-electrode assembly (MEA) was fabricated by sandwiching the Nafion 112 membrane (DuPont) between the anode and cathode by hot pressing at 130 °C and 50 kg cm^{-2} for 40 s. The geometric area of the electrodes was 5 cm^2. Pure oxygen and air were used as cathode reactants and pure H_2 as anode reactant (all gases of 99.99% purity). Stoichiometric flow rates of anode (s = 2) and cathode (s = 9.5 for O_2 and s = 2 for air) reactants were used at current densities ≥ 0.2 A cm^{-2} and constant flows (corresponding to 0.2 A cm^{-2} flows) were used at <0.2 A cm^{-2}. Reactant humidification was achieved by water-bubblers, the temperatures of which were calibrated to yield the quoted relative humidity (RH) values.

The fuel cell testing was carried out with a 5 cm^2 active area of the MEA in the PEM fuel cell test station. The experiments were staged at 70 °C. Before the

steady-state polarization curves were recorded, the cell was kept at a constant current density of 250 mA cm^{-2} for 2 h until the open circuit voltage (OCV) became steady and constant (MEA conditioning). Then, the polarization curves were recorded.

3. Results and discussions

3.1. Physical characterization of the electrocatalysts

Fig. 1 shows the XRD profile of synthesized electrocatalysts. The characteristic peaks can be well indexed as face centered cubic (fcc) crystalline. The subtle shifts of the peak positions of the XRD patterns arise from different lattice parameters for the synthesized electrocatalysts. The atomic size of Fe and Co is 156 and 152, respectively. Thus, the lattice parameters are expected to increase in the order of PtFeCo/Gr > PtFe/Gr > PtCo/Gr. In the XRD pattern of electrocatalysts, the Pt (111) plane was chosen for the calculation of the lattice parameter [20].

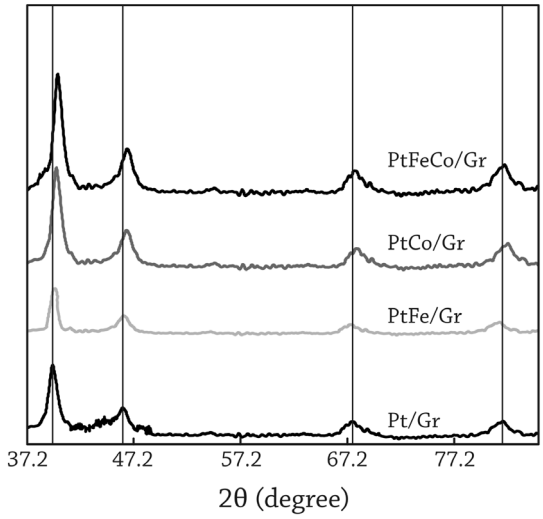

Fig. 1. XRD patterns of synthesized electrocatalysts.

The lattice parameter of PtFeCo/Gr, PtFe/Gr, PtCo/Gr and Pt/Gr are 3.852, 3.923, 3.921 and 3.948 Å, respectively, where PtFeCo/Gr does not follow this trend. This may be due to the strong magnetic moment of PtFeCo [19]. The changes of the lattice parameters are denoted as strain. The strain in the alloy is calculated using the Eq. 1 [21]:

$$S_{Pt} = \left\{ \frac{\left(a_{alloy} - a_{Pt} \right)}{a_{Pt}} \right\} \times 100 \quad (1)$$

where a_{alloy} is the lattice parameter of Pt- alloy/Gr and a_{Pt} is the lattice parameter of bulk Pt. The effect of alloying with low molar fraction of Fe and Co metals caused a higher compressive strain (2.4 %) than PtFe/Gr (0.7 %) and PtCo/Gr (0.6 %). Hence, due to the theoretical study by density functional theory (DFT), the d-band center of the alloyed Pt surface in PtFeCo/Gr shifts to a lower position with respect to the Fermi level because of the higher compressive strain and electronic effects created by the alloying metals. The down shifting of the d-band center favors the (oxygen reduction reaction) ORR activity by reducing the adsorption energy (AE) of oxygen and OH intermediates bonding to the Pt surface [22].

The crystallite size of PtFeCo/Gr, PtFe/Gr, PtCo/Gr and Pt/Gr was estimated to be 6.9, 12, 9.3 and 6.8 nm from the XRD data utilizing the Debye Scherrer equation [20].

The chemical states of the OH functionalized graphene and PtFeCo/Gr were analyzed by XPS, as depicted in Fig. 2. In the C1s deconvolution XPS spectrum, four peaks which can be assigned to non-oxygenated C at 284.6 eV, C-O at 286.6 eV, C=O at 288.2 eV, and O-C=O at 290.2 eV are observed (Fig. 2a and Fig. 2b) [23-25]. As observed, compared with that of functionalized graphene, the absorbance peaks of oxygen functionalities in XPS spectrum of PtFeCo/Gr are quite weak (Fig. 2b), indicating the effective removal of most oxygen-containing groups after the reduction process and heat treatment at 500 °C [23, 26].

The PtFeCo/Gr nanocomposite shows a double-volcano plot at a binding energy of 71.4 and 74.9 eV (Fig. 2c), which are characteristic of the Pt 4f7/2 and Pt 4f5/2 band, respectively, indicating the existence of Pt metal.

The surface core level shifts can be viewed as a measure of the variation in the d band center [27] and

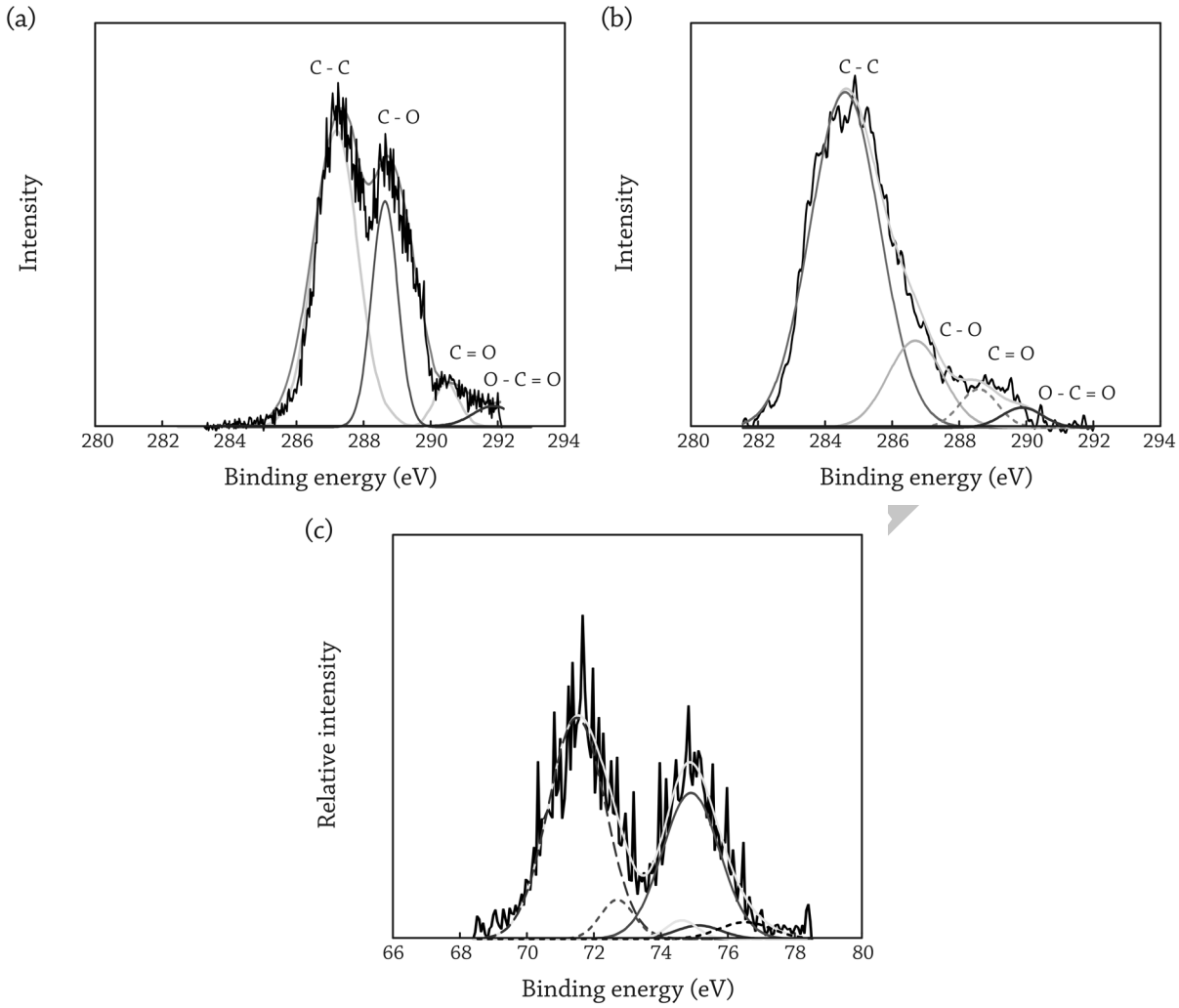

Fig. 2. C1s XPS spectra of OH functionalized graphene and PtFeCo/Gr (a, b) and Pt 4f electron spectra of PtFeCo/Gr (c).

any changes in the d-band center accompany similar variations in the surface core level shifts in the same direction [28]. So, the surface core level shifts are important parameters with respect to the chemical properties of metal surfaces. The observed binding energies for Pt are noticeably higher than that of either bulk Pt [29], Pt/C [30] or PtCo/Gr [31]. The positive shift in binding energy corresponds to a decrease in the electronic charge density on the Pt atoms in the PtFeCo/Gr catalyst, and might be due to Pt - Gr interactions and an electron shift from Pt to the graphene or due to the presence of Fe and Co in an alloy with Pt which influences the Pt d-orbital vacancy resulting in favorable d-orbital vacancy in PtFeCo/Gr for ORR. After curve fitting using the SDP software program (version 4.1) with 80% Gaussian–20% Lorentzian peak fitting, we observed that Pt contains various states such as Pt(0) (metallic Pt), Pt(II) (PtO), and Pt(IV) (PtO_2) with respective binding energies of 71.4, 72.7 and 74.6 eV and that the ratios of the various Pt states were found to be 79.3, 14.1 and 6.6. So PtO and PtO_2 reduced under the heat treatment process.

Fig. 3 presents SEM images of the synthesized electrocatalyst. In Fig. 3a nanorods of PtFe are grown on the surface of OH functionlized graphen nanosheets while spherical Pt and PtCo nanoparticles are loaded on to nanosheets (Fig. 3b, c). Interestingly, 3D rhombus shapes clusters comprising a dozen Pt alloy nanoparticles were obtained and homogenously loaded onto the graphene nanosheets (Fig. 3d).

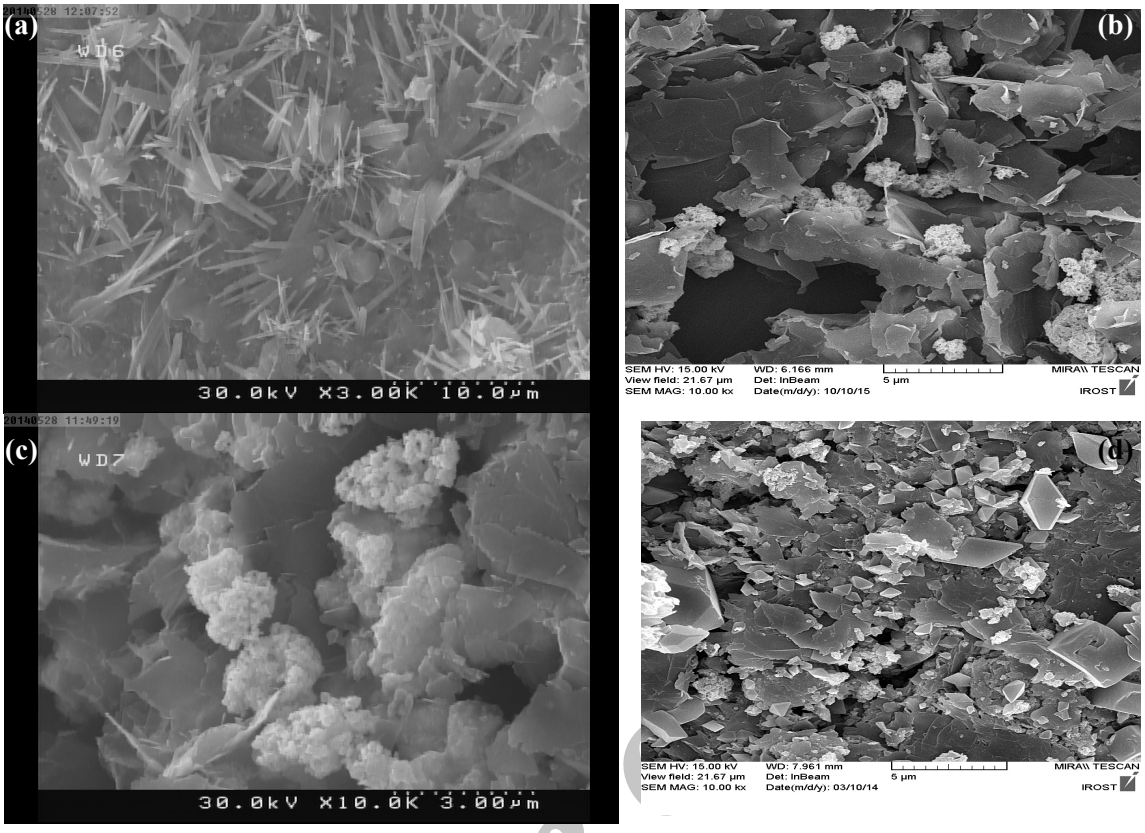

Fig. 3. SEM images of (a) PtFe/Gr, (b) Pt/Gr, (c) PtCo/Gr and (d) PtFeCo/Gr electrocatalyst.

Basically, three kinds of particles can be recognized, one is spherical, one is nanorod and another is rhombus shaped. Spherical particles may be an alloy of Pt and Co. Nanorod particles may be an alloy of Pt and Fe. The rhombus shapes clusters probably contain the PtFeCo alloy with a significantly enlarged surface area. This enlarged surface area can have a desirable impact on the formation of higher amounts of triple-contract zones (electrocatalyst/ Nafion/ gas), easier oxygen reduction reaction and higher performance of electrocatalysts. This shape transformation from Spherical -to-nanorod -to- rhombus is the result of the kinetically controlled growth [32].

The above results demonstrate that the preparation method presented herein, second and third metal addition, and their mole fractions can facilitate the establishment of Pt alloy 3D rhombus shaped nanoparticles on graphene nanosheets. The surface functional groups (such as hydroxyl groups) present in the surface of graphene nanosheets likely sever a crucial function in the formation of dispersed Pt alloy adsorption capacity and therefore on EAS can be observed. One of the reasons for this might be due to the fact that the triple-contract zones (electrocatalyst/ Nafion/ gas) are formed in a way that causes the different porosity and EAS. As pointed out the parameters, such as the electronic state of metal particles, strain between active metal atoms, the synergistic effect, the ratio of low coordinated atoms, the amount of transition metals in the electrocatalysts and permittivities in electrocatalysts, can have sever effects on the triple-contract zones (electrocatalyst/ Nafion/ gas) formation and thus on the active surface of catalysts. Fig. 4b depicts the CVs for the synthesized electrocatalysts. The hydrogen adsorption/desorption peaks can be clearly seen in the potential range between -0.3 V and 0.08 V, a double layer is observed at 0.08-0.3 V, and metal oxides formation and reduction are observed at higher potentials for the CVs. The absence of pure Fe or Co oxidation peaks indicate that the prepared samples are in true alloy states, consistent with the XRD result illustrated later. The currents for

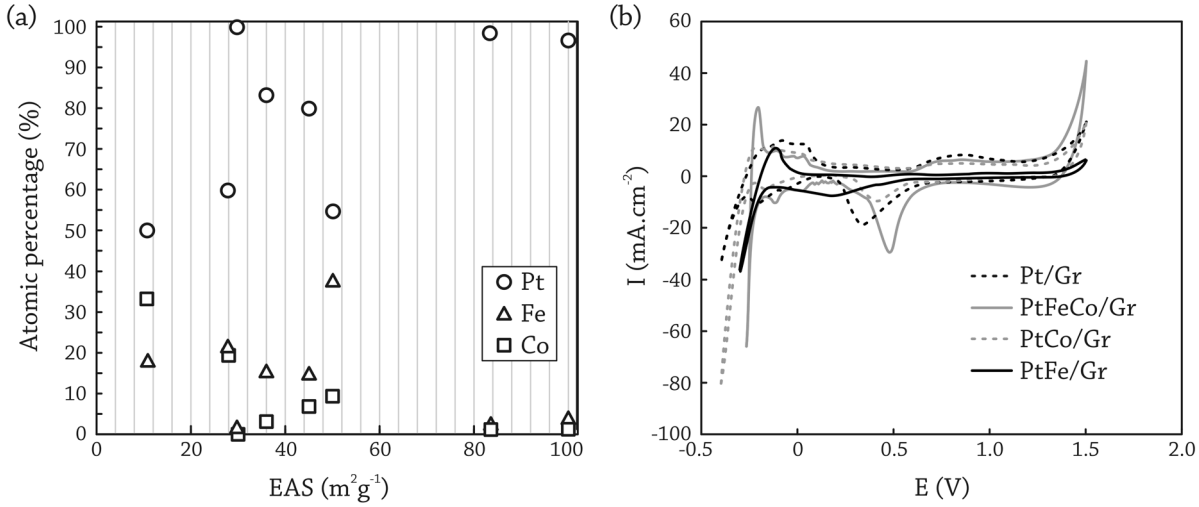

Fig. 4. (a) Pt, Fe and Co atomic percentages in PtFeCo/Gr electrocatalysts against the EAS of electrocatalysts determined by ICP- AES analysis and (b) Cyclic voltammogram of the electrocatalysts in 2M H_2SO_4 at a scan rate of 50 mV s^{-1}.

PtCoFe/Gr are higher than previously reported PtCoFe/C electrocatalyst with different composition, different carbon support and different synthesis method [9]. The EAS of the synthesized electrocatalysts follows the order PtCoFe/Gr > Pt/Gr > PtFe/Gr > PtCo/Gr. In the case of PtFe/Gr and PtCo/Gr binary alloys, the loss can be attributed to the decrease of surface Pt sites due to the substituted transition metals. At potentials lower than 0.56 V in the cathodic branch of the CVs, metals oxides undergo reduction. From Fig. 4b, it is obvious that the reduction peak for the PtCoFe/Gr electrocatalyst appears around 0.47 V, which is higher than 0.42, 0.18 and 0.33 for PtFe/Gr, PtCo/Gr and Pt/Gr, respectively. This result suggests the easiest ORR of the PtCoFe/Gr. The loss of utilization in the PtCo/Gr electrocatalyst is explained by the loss of EAS due in part to its lower lattice parameter.

Fig. 5 presents a typical set of PEM fuel cell performance data for the as-prepared MEAs. The testing was conducted at 75 ºC and atmospheric pressure. The cathodes (using synthesized PtCoFe/Gr and Pt/Gr electrocatalysts with catalyst loading of 0.1 mg cm^{-2} as catalyst) was fed with O_2, while the anodes (with Pt on carbon black from E-TEK with catalyst loading of 0.1 mg cm^{-2} Pt as catalyst) were fed with humidified H_2. The power density of the PEM fuel cell with the synthesized cathode electrocatalyst with low metal-loading (0.1 mg cm^{-2} Pt) can reach 220 mW cm^{-2} comparable to that of the PtFeCo/C (713 mW cm^{-2}) with 80% and 60% higher Pt loading in cathode and anode, respectively [9]. Fig. 5 shows that the cell performance was improved for Fig. 5 presents a typical set of PEM fuel cell performance data for the as-prepared MEAs. The testing was conducted at 75 ºC and atmospheric pressure. The cathodes (using synthesized PtCoFe/Gr and Pt/Gr electrocatalysts with catalyst loading of 0.1 mg cm^{-2} as catalyst) was fed with O_2, while the anodes (with Pt on carbon black from E-TEK with catalyst loading of 0.1 mg cm^{-2} Pt as catalyst) were fed with humidified H_2. The power density of the PEM fuel cell with the synthesized cathode electrocatalyst with low metal-loading (0.1 mg cm^{-2} Pt) can reach 220 mW cm^{-2} comparable to that of the PtFeCo/C (713 mW cm^{-2}) with 80% and 60% higher Pt loading in cathode and anode, respectively [9]. Fig. 5 shows that the cell performance was improved for MEA with PtCoFe/Gr as the cathode electrocatalyst. This result can be attributed to a larger EAS and higher ORR activity.

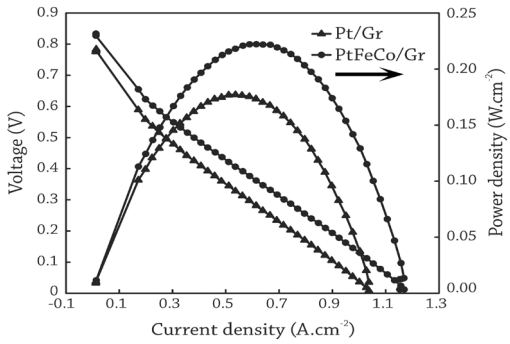

Fig. 5. Polarization curves for a membrane electrode assembly containing the Pt/Gr and PtFeCo/Gr electrocatalysts as the cathode and commercial Pt/C catalyst as the anode, with a cathode catalyst loading of 0.1 mg cm^{-2} at 75ºC operated with humidified H_2/O_2 gases without any back pressure.

4. Conclusions

In summary, 3D rhombus shaped clusters comprising a dozen PtCoFe nanoparticles homogeneously dispersed on graphene nanosheets were synthesized. Pt/Gr, PtFe/Gr and PtCo/Gr were also synthesized for comparison. It was observed that the preparation method presented herein, second and third metal addition, and their mole fractions can facilitate the establishment of Pt alloy 3D rhombus shapes nanoparticles on graphene nanosheets. Incorporation of the less expensive Fe and Co into Pt in a PtCoFe/Gr ternary electrocatalyst can reduce the overall cost of the catalyst and effectively enhance compressive strain. Therefore, due to the theoretical study by density functional theory, the d-band center of the alloyed Pt surface in PtFeCo/Gr shifted to a lower position with respect to the Fermi level (because of the higher compressive strain and electronic effects created by the alloying metals) and this down shifting of the d-band center favors the ORR activity by reducing the adsorption energy of oxygen and OH intermediates bonding to the Pt surface. Thus, PtCoFe/Gr ternary electrocatalyst enhances ORR activity by shifting the half-wave potential to more positive potentials by about 0.1 V and offers significant cost to performance benefits. Fuel cell tests showed that the cell performance was improved for MEA with PtCoFe/Gr as the cathode electrocatalyst. This result can be attributed to a larger EAS and higher ORR activity. The greatly improved EAS, ORR activity and cell performance is achieved by increasing the utilization of the PtCoFe/Gr electrocatalyst by enhancing the three-phase boundary in the catalyst layer.

Acknowledgments

This work was carried out in the Renewable Energy Research Center of Amirkabir University of Technology. The authors thank all who assisted in this work.

5. References

[1] Wang R., Higgins D. C., Hoque M. A., Lee D. U., Hassan F., et al., "Controlled growth of platinum nanowire arrays on sulfur doped graphene as high performance electrocatalyst" , Sci. Rep., 2013, 3: 2431.

[2] Carpenter M.K., Moylan T.E., Kukreja R.S., Atwan M.H., Tessema M.M., "Solvothermal Synthesis of Platinum Alloy Nanoparticles for Oxygen Reduction Electrocatalysis", J. Am. Chem. Soc., 2012, 134: 8535.

[3] Yang L.F., Shan S.Y., Loukrakpam R., Petkov V., Ren Y., et al., "Role of Support–Nanoalloy Interactions in the Atomic-Scale Structural and Chemical Ordering for Tuning Catalytic Sites", J. Am. Chem. Soc., 2012, 134: 15048

[4] Javaheri M., "Using the palladium as core and platinum as shell for ORR", Iranian Journal of Hydrogen & Fuel Cell, 2014, 3: 133-139.

[5] Hoshyar N., Irankhah A., "Effect of platinum on ceria supported copper catalysts for PrOx process in fuel processors", Iranian Journal of Hydrogen & Fuel Cell, 2014, 1: 47-53.

[6] Kheirmand M., Rastegari F., "Oxygen reduction reaction on Pt/C at the presence of super paramagnetic of Fe_3O_4

nanoparticles for PEMFCs", Iranian Journal of Hydrogen & Fuel Cell, 2014, 1: 41-45.

[7] Malheiro A.R., Perez J., Villullas H. M., "Dependence on composition of electronic properties and stability of Pt–Fe/C catalysts for oxygen reduction", J. Power Sources, 2010, 195: 7255-7260.

[8] Neetu J., Imran Jafri R., Rajalakshmi N., Ramaprabhu S., "Graphene-multi walled carbon nanotube hybrid electrocatalyst support material for direct methanol fuel cell", Int. J. Hydrogen Energy, 2011, 36: 7284-7290.

[9] Karuppannan M., Louis C., "Impact of alloying and lattice strain on ORR activity of Pt and Pd based ternary alloys with Fe and Co for proton exchange membrane fuel cell applications", RSC Adv, 2014, 4: 11939-11947.

[10] Antolini E., "Platinum-based ternary catalysts for low temperature fuel cells: Part II. Electrochemical properties", Appl. Catal., B: Environmental, 2007, 74: 337–350.

[11] Bose S., Kuila T., Mishra A.K., et al, "Dual role of glycine as a chemical functionalizer and a reducing agent in the preparation of graphene: an environmentally friendly method", J Mater Chem, 2012, 22: 9696.

[12] Kakaei K., Gharibi H., Abbaspour S., "One –step synthesis of PdCo alloy nanoparticles decorated on reduced grahene oxide as an Electro-catalyst for Oxygen Reduction Reaction in Passive Direct Methanol Fuel Cells", Iranian Journal of Hydrogen & Fuel Cell, 2015, 2(1): 27.

[13] Kheirmad M., Eshghi A., "Electrodeposition of platinum nanoparticles on reduced graphene oxide as an efficient catalyst for oxygen reduction reaction", Iranian Journal of Hydrogen & Fuel Cell, 2015, 2(1): 7.

[14] Ghanbarlou H., Rowshanzamir S., Parnian M. J., et al, "Preparation of Nitrogen-Doped Graphene By Solvothermal Process as Supporting Material for Fuel Cell Catalysts", Iranian Journal of Hydrogen & Fuel Cell, 2014, 1(2): 113.

[15] Stankovich S., Dikin D. A., Dommett G. H. B., et al, "Graphene-based composite materials", Nature, 2006, 442: 282.

[16] Lee C., Wei X., Kysar J. W., et al, "Measurments of the elastic properties and intrinsic strength of monolayer grapheme", Science, 2008, 321: 385.

[17] Geim A. K., "Graphene: Status and Prospects", Science, 2009, 324: 1530.

[18] Lee S. H., Kakati N., Jee S. H., Maiti J., Yoon Y. S., "Hydrothermal synthesis of PtRu nanoparticles supported on graphene sheets for methanol oxidation in direct methanol fuel cell", Mater. Lett., 2011, 65: 3281.

[19] Venkateswara R.Ch, Viswanathan B., J. Phys. Chem. C, 2010, 114: 8661–7.

[20] Cality B. D, "Elements of X-ray Diffraction" Addision-Wesley Publishing Company, INC, 1956.

[21] Wang J., Huang J., Duan H., Yu S., Feng X., et al., "Surface stress effect in mechanics of nanostructured materials" Acta Mech Sinica, 2011, 24: 52.

[22] Strasser P., Koh S., Anniyev T., et al., "The preparation of stable metal nanoparticles", Nature, 2010, 2: 454.

[23] Tang L. H., Wang Y., Li Y. M., et al., "Preparation, structure, and electrochemical properties of reduced graphene sheet films", Adv. Funct. Mater., 2009, 19(17): 2782.

[24] Geng H. Z., Kim K. K., Song C., et al., "Doping and de-doping of carbon nanotube transparent conducting films by dispersant and chemical treatment" J. Mater. Chem., 2008, 18(11): 1261.

[25] Akhavan O., Ghaderi E., "Photocatalytic reduction of graphene oxide nanosheets on TiO2 thin film for photoinactivation of bacteria in solar light irradiation", J. Phys. Chem. C, 2009, 113(47): 20214.

[26] Li X. L., Zhang G. Y., Bai X. D, et al., "Highly

conducting graphene sheets and Langmuir-Blodgett films", Nat. Nanotechnol., 2008, 3(9): 538.

[27] Hammer B., Nørskov J.K., "Theoretical Surface Science and Catalysis- Calculations and Concepts", Advances in Catalysis, 2000: 45.

[28] Allen G. C., Tucker P. M., Capon A., Parsons R., "X-ray photoelectron spectroscopy of adsorbed oxygen and carbonaceous species on platinum electrodes", J. Electroanal. Chem., 1974: 50, 335.

[29] Hull R., Li L., Xing Y., Chusuei C., " Pt Nanoparticle Binding on Functionalized Multiwalled Carbon Nanotubes", Chem. Mater, 2006, 18: 1780.

[30] Zhang L., Zhen W., Jing Z., Xu S., Lei Z., " Honeycomb-like mesoporous nitrogen-doped carbon supported Pt catalyst for methanol electrooxidation", Carbon, 2015, 93: 1050.

[31] Yan M., Zhong L., Bo W., Le Z., Jian Y., et al.," Preparation of graphene-supported Pt-Co nanoparticles and their use in oxygen reduction reactions", New Carbon Mater, 2012, 27: 250.

[32] Petroski J. M., Wang Z. L., Green T. C., El-Sayed, M. A., "Shape Transformation and Melting of Cubic and Tetrahedral Platinum Nanocrystals ", J. Phys. Chem. B 1998 , 10 , 3316.

[33] Pozio A., Francesco M. D., Cemmi A., et al, "Comparison of high surface Pt/C catalysts by cyclic voltammetry", J. Power Sources, 2002, 105: 13.